



## On stability of self-assembled nanoscale patterns

Shaowen Hu<sup>a,1</sup>, Girish Nathan<sup>b</sup>, Fazle Hussain<sup>c</sup>,  
Donald J. Kouri<sup>a,b,d</sup>, Pradeep Sharma<sup>b,c,\*</sup>,  
Gemunu H. Gunaratne<sup>b,e,\*</sup>

<sup>a</sup>Department of Chemistry, University of Houston, Houston, TX 77204, USA

<sup>b</sup>Department of Physics, University of Houston, Houston, TX 77204, USA

<sup>c</sup>Department of Mechanical Engineering, University of Houston, Houston, TX 77204, USA

<sup>d</sup>Department of Mathematics, University of Houston, Houston, TX 77204, USA

<sup>e</sup>The Institute for Fundamental Studies, Kandy, Sri Lanka

Received 17 August 2006; received in revised form 22 December 2006; accepted 15 January 2007

---

### Abstract

We conduct linear and nonlinear stability analyses on a paradigmatic model of nanostructure self-assembly. We focus on the spatio-temporal dynamics of the concentration field of deposition on a substrate. The physical parameter of interest is the mean concentration  $C_0$  of the monolayer. Linear stability analysis of the system shows that a homogeneous monolayer is unstable when  $C_0$  lies within a band symmetric about  $C_0 = \frac{1}{2}$ . On increasing  $C_0$  from zero, the homogeneous solution destabilizes to a hexagonal array, which then transitions to stripes. Transitions to and from the hexagonal state are subcritical. Square patterns are unstable for all values of  $C_0$  transitioning either to hexagons or stripes. Further, we present stability maps for striped arrays by considering possible instabilities. The analytical results are confirmed by numerical integrations of the Suo–Lu model. Our formalism provides a theoretical framework to understand guided self-assembly of nanostructures.

© 2007 Elsevier Ltd. All rights reserved.

*Keywords:* Self-assembly; Stability analysis; Nanostructures

---

---

\*Corresponding authors. Tel.: +1 713 743 4256.

E-mail addresses: [psharma@uh.edu](mailto:psharma@uh.edu) (P. Sharma), [gemunu@uh.edu](mailto:gemunu@uh.edu) (G.H. Gunaratne).

<sup>1</sup>Current address: Division of Space Life Sciences, USRA/NASA-JSC, 3600 Bay Area Blvd., Houston, TX 77058, USA.

## 1. Introduction

Self-assembly, i.e., the spontaneous formation of patterns (Whitesides and Grzybowski, 2002), is emerging as a promising technique for epitaxial growth of regular nanoscale arrays on a substrate. For example, Pohl et al. (1999) observed that when a monolayer of silver deposited on a ruthenium (001) surface is exposed to sulfur, a regular array of 3.4 nm diameter (sulfur) disks is formed; Wahlström et al. (1999) showed that the deposition of sulfur on Cu (111) substrate at low temperature leads to the formation of honeycomb-like structures with a length scale of 1.67 nm; Umezawa et al. (2001) reported the growth of a network of equilateral triangles of side 3 nm when a Ag monolayer of fractional coverage 0.8 is deposited on Cu (111) substrate at room temperature.

At the scale of interest, each of the above experimental systems is (nearly) isotropic and homogeneous and the epitaxial deposition is spatially homogeneous except for stochastic effects. The destabilization of the homogeneous monolayer is caused by spontaneous symmetry breaking giving energetically favorable patterned structures (Cross and Hohenberg, 1993). Although detailed microscopic theories are needed to predict quantitative features of surface structures for a given experimental configuration, general characteristics of self-assembly can be studied using phenomenological field theoretic models. Factors that need to be included in such models are: (i) a double-welled free energy function of the epilayer to ensure phase separation; (ii) an interfacial energy between distinct monolayer phases; and (iii) an elastic energy due to non-uniformity of the surface stress (Ng and Vanderbilt, 1995; Glas, 1997; Guyer and Voorhees, 1998; Suo and Lu, 2000). The competition between (ii) and (iii) is responsible for size selection of self-assembled domains. The relative simplicity of the phenomenological models allows one to conduct a comprehensive theoretical analysis of self-assembled states, their stability domains, and how they destabilize.

Our studies are conducted on a Cahn–Hilliard type model of self-assembly due to Suo and Lu (2000) which is introduced briefly in Section 2. The physical variable of interest is the mean fractional coverage  $C_0$  of the monolayer and the remaining parameters, such as the elastic mismatch and temperature, are kept fixed. Stability boundaries for the homogeneous solution are evaluated in Section 3 using linear stability analysis. Consistent with previous variational calculations, the homogeneous solution is unstable for an interval  $I$  symmetric about  $C_0 = \frac{1}{2}$ . Section 4 shows examples of hexagonal, striped and labyrinthine structures generated in numerical integrations of the model system while their stability maps are calculated using nonlinear stability analysis in Section 5. In Sections 6–8, we present the major new contributions of our work, namely *nonlinear* stability analyses of striped, square and hexagonal arrays using multiple scales analysis (Newell and Whitehead, 1969; Segel, 1969; Cross and Hohenberg, 1993). In particular, we show in Section 7 that square arrays are never stable, and in Sections 6 and 8 calculate stability boundaries for striped and hexagonal arrays. Theoretical results for striped arrays are shown to agree very well with those from numerical integrations of the Suo–Lu model. Agreement for the hexagonal case, although close, is imperfect. We argue that this disagreement is due to the finite amplitude of the hexagonal structures for parameter values considered in the paper. Section 9 discusses the merit of our work in providing a theoretical framework for guiding self-assembly of nanostructures.

Linear and nonlinear stability analysis have several advantages over techniques based on calculating the energy of a given collection of solutions. It does not require the underlying

system to be variational. Further, the instability of a given solution can be determined without prior knowledge of the state to which it destabilizes. These considerations are important in calculating the stability boundaries of periodic arrays.

## 2. A thermodynamic model of self-assembly

The phenomenological model of Suo and Lu (2001) contain components that are energetically most relevant for self-assembly in a two-species system: phase separation, phase coarsening, and phase refining. Due to the mismatch in surface stress between adjoining phases, both the monolayer and the substrate are elastically stressed. The spatio-temporal dynamics for the concentration field  $C(x, y)$  of the epilayer atoms (Lu and Suo, 2001) was shown to be

$$\frac{\partial C}{\partial t} = \frac{M}{A^2} \nabla^2 \left( \frac{\partial g}{\partial C} - 2h_0 \nabla^2 C + \phi \varepsilon_{\beta\beta} \right), \quad (1)$$

where the parameters  $M$ ,  $A$ ,  $h_0$ , and  $\phi$  represent, respectively, the atomic mobility in the monolayer, the number of substrate atomic sites per unit area, the energy contribution due to concentration gradients, and the rate of change of the surface stress with respect to concentration.

The function  $g = g(C)$  is the excess energy per unit area and depends on the presence (represented by species B) or absence (represented by species A) of the epilayer atoms at a substrate site. Its dependence on the concentration of the epilayer is

$$g(C) = g_A(1 - C) + g_B C + AkT[C \ln C + (1 - C) \ln(1 - C) + \Omega C(1 - C)], \quad (2)$$

where  $g_A$  and  $g_B$  are the excess energy of the fully occupied and the fully vacant epilayer.  $k$  denotes Boltzmann's constant and  $T$  the absolute temperature. The first two terms in brackets give the entropy of mixing and the third term the energy of mixing. The dimensionless parameter  $\Omega$  measures the exchange energy relative to the thermal energy  $kT$ .  $g(C)$  is of the form (2) as long as the epilayer obeys the regular solution theory (Cahn and Hilliard, 1958). Phase separation occurs only if  $g(C)$  is non-convex, or equivalently if  $\Omega > 2$  (Suo and Lu, 2001).

The second term on the right side of Eq. (1) represents energy associated with a phase boundary. If  $h_0 > 0$ , any nonuniformity in the concentration field increases the surface free energy. Hence, the phase boundary energy is reduced by increasing domain sizes, i.e., by phase coarsening.

$\varepsilon_{\beta\beta}$ , the concentration-dependent elastic strain, is given by

$$\varepsilon_{\beta\beta} = -\frac{(1 - \nu^2)\phi}{\pi E} \iint \frac{(x - \xi_1)\partial C/\partial \xi_1 + (y - \xi_2)\partial C/\partial \xi_2}{[(x - \xi_1)^2 + (y - \xi_2)^2]^{3/2}} d\xi_1 d\xi_2, \quad (3)$$

where  $E$  and  $\nu$  are the substrate's Young's modulus and Poisson's ratio, and the integration extends over the entire surface.  $\varepsilon_{\beta\beta} = 0$  for a homogeneous solution, but can be negative for suitably chosen non-constant  $C(x, y)$ . Thus, phase refining can reduce  $\varepsilon_{\beta\beta}$ . Note that Eq. (3) assumes isotropic elasticity.

The first two terms in Eq. (1) are similar to those in spinodal decomposition (Cahn and Hilliard, 1958). Numerical simulation confirms that, in the absence of phase refining, the dynamics of the Suo–Lu model reproduces the classical spinodal decomposition (Lu and Suo, 2002). In model (1), the surface strain saturates unbounded growth of domains.

Eq. (1) can be rescaled into a dimensionless form by scaling the spatial coordinates by  $\sqrt{h_0/\Lambda kT}$  and time by  $h_0/M(kT)^2$ , giving

$$\frac{\partial C}{\partial t} = \nabla^2 \left\{ P(C) - 2\nabla^2 C - \frac{Q}{\pi} I_0 \right\}, \tag{4}$$

where

$$P(C) = \ln \left( \frac{C}{1-C} \right) + \Omega(1-2C), \tag{5}$$

$$I_0 = \iint \frac{(x-\xi_1)\partial C/\partial \xi_1 + (y-\xi_2)\partial C/\partial \xi_2}{[(x-\xi_1)^2 + (y-\xi_2)^2]^{3/2}} d\xi_1 d\xi_2, \tag{6}$$

and  $Q = b/l$  is the ratio of the typical ‘‘width’’  $b = (h_0/\Lambda kT)^{1/2}$  of domains and the characteristic thickness  $l = Eh_0/(1-v^2)\phi^2$  of an interface between two phases. For most epitaxial systems, both  $b$  and  $l$  are of order of 1 nm.

### 3. Linear stability analysis

The stability analysis for the homogeneous solution of the Suo–Lu model has been conducted previously by considering changes in the surface free energy caused by small sinusoidal perturbations (Lu and Suo, 1999; Suo and Lu, 2001). For completeness, we outline a more general linear stability analysis that does not require the system to be variational (Walgraef, 1997).

Consider a perturbation of the homogeneous solution  $C(x, y) = C_0$  of the form

$$C(x, y) = C_0 + ze^{iqx+\sigma t} \tag{7}$$

with  $z \ll C_0$ . At the lowest order

$$\nabla^2 P(C) = -q^2 \left( \frac{1}{C_0(1-C_0)} - 2\Omega \right) ze^{iqx+\sigma t}. \tag{8}$$

As shown in Appendix A,  $I_0$  is the convolution of derivatives of  $\rho^{-1} = (x^2 + y^2)^{-1/2}$  and  $C(x, y)$ . Thus,

$$\begin{aligned} \nabla^2 I_0 &= -\nabla^2 \left( \frac{\partial \rho^{-1}(x, y)}{\partial x} * \frac{\partial ze^{iqx+\sigma t}}{\partial x} \right) \\ &= -q^4 \rho^{-1}(x, y) * ze^{iqx+\sigma t} \\ &= -q^4 \iint \rho^{-1}(\xi_1, \xi_2) \times ze^{\sigma t} e^{iq(x-\xi_1)} d\xi_1 d\xi_2 \\ &= -q^4 ze^{iqx+\sigma t} \iint \rho^{-1}(\xi_1, \xi_2) e^{-iq\xi_1} d\xi_1 d\xi_2 \\ &= -2\pi q^3 z^{iqx+\sigma t}. \end{aligned} \tag{9}$$

Note that the last step uses the Fourier–Bessel transform (Bracewell, 1999).

Denoting  $h_1 = 1/C_0(1-C_0) - 2\Omega$ , the growth rate becomes

$$\sigma = -2q^2 \left[ \frac{h_1}{2} - Qq + q^2 \right]. \tag{10}$$

Unless  $\sigma(q)$  is zero or negative for all  $q$ , the uniform state  $C(x, y) = C_0$  is unstable to small perturbations. Clearly,  $h_1$ , and hence  $C_0$ , determines the threshold of the instability. The critical concentration is  $h_c = Q^2/2$ . At parameters used by Suo and Lu (2001) ( $Q = 1.0$  and  $\Omega = 2.2$ ), the homogeneous solution destabilizes for  $C_0 \in [0.29, 0.71]$  symmetric about  $C_0 = \frac{1}{2}$ . Self-assembly will be observed only within this interval (except for a small parameter range where both the hexagonal state and the homogeneous solution are stable, see Section 8). The dispersion relation is given by

$$\sigma = 2q^2[r - (q - Q/2)^2], \tag{11}$$

where

$$\begin{aligned} r &= (h_c - h_1)/2 \\ &= \frac{Q^2}{4} - \frac{1}{2C_0(1 - C_0)} + \Omega. \end{aligned} \tag{12}$$

The results of the linear stability analysis are identical to those obtained from energy minimization (Suo and Lu, 2001).

Near the onset of patterns, the critical wavenumber  $q_c = Q/2$ , and the corresponding wavelength is  $4\pi/Q$ . The marginal stability condition and the linear growth rates of perturbations are shown in Fig. 1. From Eq. (10), the fastest growing mode is given by

$$q_{\text{peak}} = \frac{3Q + \sqrt{9Q^2 - 16h_1}}{8} = \frac{3Q + \sqrt{32r + Q^2}}{8}. \tag{13}$$

Note that as  $r$  increases, so does  $q_{\text{peak}}$ , and the typical lengthscale associated with the pattern decreases.

#### 4. Patterns in the Suo–Lu model

It is clear from Eq. (13) that the length scale of patterns generated in the Suo–Lu system depends on  $Q$  and  $h_1$ . Fig. 2 shows hexagonal patterns formed at  $Q = 0.8$  and 1.1. As discussed in the previous Section, increasing  $Q$  reduces the nearest neighbor distance.

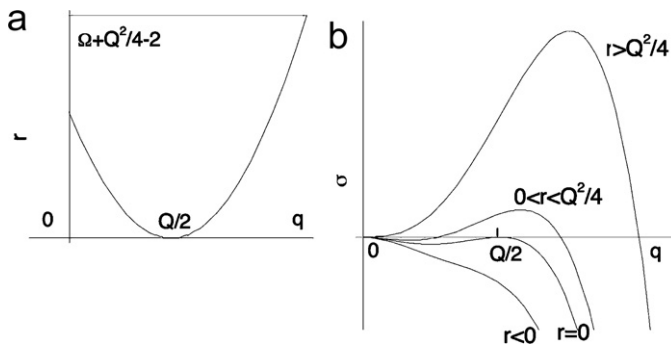


Fig. 1. (a) The marginal stability curve, above which the homogeneous state is unstable to small perturbation. The horizontal line on top is the peak value  $\Omega + Q^2/4 - 2$  of  $r$ . (b) The linear growth rates of small amplitude Fourier modes. Note that the  $q = 0$  mode is marginal for all  $r$ . For  $r < 0$  all other modes decay, while for  $0 < r < Q^2/4$  there is a band of Fourier modes about  $Q/2$  that grow. For  $r > Q^2/4$  the band of growing modes includes the  $q = 0$  mode.

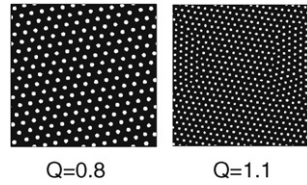


Fig. 2. Patterns at  $t = 315985$  for systems with the same mean concentrations  $C_0 = 0.31$  and  $\Omega = 2.2$ , but with different values of  $Q$ . The increase of  $q$  where the peak of the dispersion relation is located is reflected in the reduction of the lengthscale in the pattern as  $Q$  is increased. The broadening of the band of unstable Fourier modes implies that, typically, the textures are more disordered for large  $Q$ . Integrations are implemented on a square domain of  $256 \times 256$  lattice points with periodic boundary conditions. Each side of the domain is  $256l$ .

In addition, it is seen that the typical disorder in a pattern increases with  $Q$ . This behavior is easily explained by noting that for fixed  $C_0$ ,  $r$  increases with  $Q$ . Near the onset, only a narrow band of Fourier modes are excited, and hence the domain sizes are large (Cross and Hohenberg, 1993). In contrast, for larger  $r$  the band of growing Fourier modes is broader and, in addition, nonlinear terms in the model are larger; consequently, textures in such systems are more disordered. This is a common feature of pattern formation (Manneville, 1990).

Controlling the size and homogeneity of the droplets is extremely important in fabricating nanostructures for electronic and optical devices since irregularities in textures cause inhomogeneities in these physical properties. As discussed above, linear stability analysis shows that the most ordered structures form close to the transition from the homogeneous solution to the hexagonal phase, i.e., when  $r$  is only slightly above 0.

Using the semi-implicit spectral method, we numerically integrate Eq. (4) to determine the self-assembled structures starting from random initial states (Fig. 3) for different  $C_0$ 's. Note that many qualitative features in these textures are reminiscent of those observed in experiments on chemical vapor deposition (Pohl et al., 1999; Plass et al., 2001); in particular, the order of appearance of various planforms with increasing  $C_0$  is identical to that in the well-studied Pb/Cu surface alloy experiments (Plass et al., 2001). When  $C_0 \in [0.29, 0.42]$ , only states with hexagonal droplets are observed; as  $C_0$  is increased, coexisting structures of hexagons and stripes and then only striped labyrinthine patterns are seen. Beyond  $C_0 = 0.5$  droplets of the opposite phase (B-rich as opposed to A-rich) begin to appear and their density increases with  $C_0$ . This symmetry in the type of droplets is observed in experiments as well (Plass et al., 2001).

Numerical integrations of the Suo–Lu model confirms the theoretically derived expression for the growth rate  $\sigma$  as a function of  $C_0$ ,  $Q$ , and  $\Omega$ . We also verified that self-assembly can occur only in system with positive  $r$ .

## 5. Nonlinear stability analysis

Linear stability analysis can provide instabilities only of the homogeneous solution. Nonlinear stability analysis is needed theoretically to determine the types of structures (e.g., hexagonal, square, striped or labyrinthine) that are expected beyond the transition, and to calculate their stability maps. As shown below, our results can be used to explain many features of textures seen in the Suo–Lu model.

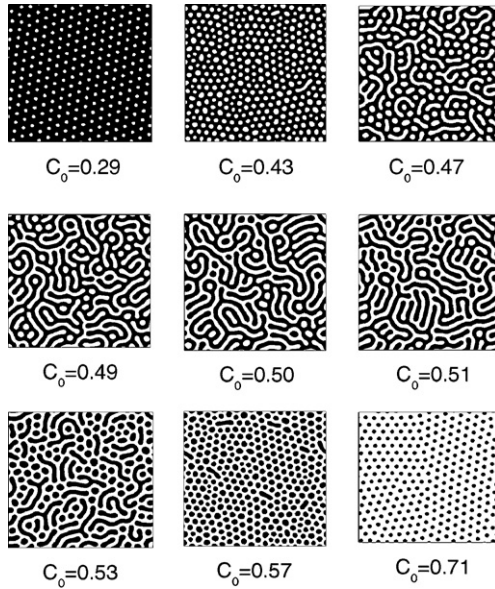


Fig. 3. The patterns at  $t = 1\,132\,234$  for systems with nine different fractional coverages ( $Q = 1.0$ , and  $\Omega = 2.2$ ). The order in which these patterns appear is the same as that for several experiments on vapor deposition.

The dispersion relation Eq. (11) has a marginal mode at  $q = 0$  reflecting the conservation of the total number of particles on the monolayer (Matthews and Cox, 2000). As  $C_0$  is increased a second mode crosses the  $\sigma = 0$  axis (at  $q = Q/2$ ) giving birth to patterned structures. Close to the onset all other modes have negative growth rates. The two marginal modes will dominate the dynamics of the system (Haken, 1987) following the adiabatic relaxation of decaying modes. It is possible to derive reduced amplitude equations for the dynamics of the marginal modes. They can be analyzed to explain many characteristics of the spatio-temporal dynamics.

### 5.1. Multiple scales analysis

According to Eq. (11), the uniform state of a system close to the onset of patterns is unstable only to perturbations with wavenumbers near  $q_c = Q/2$ . Consequently, the field  $C(x, y)$  can be expanded as

$$C(\mathbf{x}, t) = C_0 + \sum_n [A_n(\mathbf{x}, t)e^{i\mathbf{q}\cdot\mathbf{x}} + \text{c.c.}] + \dots, \tag{14}$$

where  $|\mathbf{q}| = q_c$  and  $C_0 = \langle C(x, y) \rangle$ . Note that the expansion only contains modes near  $\mathbf{q}$ , and hence the envelope functions  $A_i(x, t)$  consist only of modes with small wave-vectors; in other words, the envelope functions change very slowly in space and time (Newell and Whitehead, 1969; Segel, 1969). The standard technique to derive the spatio-temporal dynamics of the envelope functions is to write

$$C(\mathbf{x}, t) = C_0 + \varepsilon C_1 + \varepsilon^2 C_2 + \varepsilon^3 C_3 + \dots, \tag{15}$$

where the (small) parameter  $\varepsilon$  is related to the distance  $r$  to the instability via the expansion

$$r = \varepsilon r_1 + \varepsilon^2 r_2 + \varepsilon^3 r_3 + \dots \tag{16}$$

Since variations in  $A_i(\mathbf{x}, t)$  occur on a scale much larger than the basic scale ( $2\pi/q_c$ ), a set of slow variables can be introduced and the spatial and temporal derivatives are expressed as

$$\partial_t \rightarrow \varepsilon \partial_{\tau_1} + \varepsilon^2 \partial_{\tau_2} + \dots, \tag{17}$$

$$\nabla \rightarrow \nabla_0 + \varepsilon \nabla_1, \tag{18}$$

where  $\nabla_0 = (\hat{\mathbf{x}}\partial_x + \hat{\mathbf{y}}\partial_y)$  operates on the ‘‘fast’’ variables  $e^{i\mathbf{q}\cdot\mathbf{x}}$  whereas  $\nabla_1 = (\hat{\mathbf{x}}\partial_X + \hat{\mathbf{y}}\partial_Y)$  acts on the slowly varying envelope functions. Note that we have used the fact that aspects of a pattern at different scales can evolve with distinct time scales. The expansion given for  $\partial_t$  is used to separate them (Newell and Whitehead, 1969; Segel, 1969).

Defining  $\hat{\mathbf{x}}$  to be normal to the striped array and hence setting no fast variation in the  $\hat{\mathbf{y}}$  direction (Cross and Hohenberg, 1993, p. 1080), the linear terms in Eq. (4) can be expanded as

$$\begin{aligned} LC &= \nabla^2 \left( -2\nabla^2 C + \frac{Q}{\pi} I_0 \right) \\ &= \nabla^2 \left( -2\nabla^2 C + \frac{Q}{\pi} I_a \right) \\ &\rightarrow (\nabla_0^2 + 2\varepsilon \nabla_0 \nabla_1 + \varepsilon^2 \nabla_1^2) [-2(\nabla_0^2 + 2\varepsilon \nabla_0 \nabla_1 + \varepsilon^2 \nabla_1^2) C \\ &\quad + \frac{Q}{\pi} (\nabla_0 + \varepsilon \nabla_1) \rho^{-1} * (\nabla_0 + \varepsilon \nabla_1) C]. \end{aligned} \tag{19}$$

A function of  $x$  and  $y$ ,  $\rho^{-1}$  depends only on the fast variables. As the derivative of a convolution is equal to the convolution of either function with the derivative of the other (Thibos, 2003), we have

$$\nabla_0 \rho^{-1} * (\nabla_0 + \varepsilon \nabla_1) C = \rho^{-1} * (\nabla_0^2 + \varepsilon \nabla_0 \nabla_1) C. \tag{20}$$

Then

$$\begin{aligned} LC &= \nabla_0^2 H_0 C + \varepsilon [\nabla_0^2 H_1 C + 2\nabla_0 \nabla_1 H_0 C] \\ &\quad + \varepsilon^2 (-2\nabla_0^2 \nabla_1^2 C + 2\nabla_0 \nabla_1 H_1 C + \nabla_1^2 H_0 C) \\ &\quad + \varepsilon^3 (-4\nabla_0 \nabla_1 \nabla_1^2 C + \nabla_1^2 H_1 C) + \dots, \end{aligned} \tag{21}$$

where

$$H_0 = -2\nabla_0^2 + \frac{Q}{\pi} \rho^{-1} * \nabla_0^2, \tag{22}$$

$$H_1 = -4\nabla_0 \nabla_1 + \frac{Q}{\pi} \rho^{-1} * \nabla_0 \nabla_1. \tag{23}$$

The Taylor expansion of the nonlinear term is

$$\begin{aligned} \nabla^2 P(C) &= (\nabla_0^2 + 2\varepsilon \nabla_0 \nabla_1 + \varepsilon^2 \nabla_1^2) P(C) \\ &= \varepsilon (\nabla_0^2 h_1 C_1) + \varepsilon^2 [\nabla_0^2 (h_1 C_2 + h_2 C_1^2) + 2\nabla_0 \nabla_1 h_1 C_1] \\ &\quad + \varepsilon^3 [\nabla_0^2 (h_1 C_3 + 2h_2 C_1 C_2 + h_3 C_1^3) + 2\nabla_0 \nabla_1 (h_1 C_2 + h_2 C_1^2) + \nabla_1^2 h_1 C_1] \\ &\quad + \varepsilon^4 [\nabla_0^2 (h_1 C_4 + h_2 (C_2^2 + 2C_1 C_3) + 3h_3 C_1^2 C_2 + h_4 C_1^4) \\ &\quad + 2\nabla_0 \nabla_1 (h_1 C_3 + 2h_2 C_1 C_2 + h_3 C_1^3) + \nabla_1^2 (h_1 C_2 + h_2 C_1^2)] + \dots, \end{aligned} \tag{24}$$

where

$$h_1 = \frac{1}{C_0(1 - C_0)} - 2\Omega, \quad (25)$$

$$h_2 = -\frac{1}{2C_0^2} + \frac{1}{2(1 - C_0)^2}, \quad (26)$$

$$h_3 = \frac{1}{3C_0^3} + \frac{1}{3(1 - C_0)^3}, \quad (27)$$

$$h_4 = -\frac{1}{4C_0^4} + \frac{1}{4(1 - C_0)^4}. \quad (28)$$

By substituting these expressions in Eq. (4) and separating different orders in  $\varepsilon$ , one obtains the spatio-temporal dynamics for striped, square and hexagonal arrays (Appendix B).

### 5.2. Newell–Whitehead–Segel equations

The multiple scales analysis described above provides equations to describe spatio-temporal dynamics of the envelope functions for striped, square, and hexagonal structures. Below, we denote the (complex) envelope functions for critical  $\mathbf{q}$ -vectors by  $A(x, t)$ . Since the  $\mathbf{q} = 0$  mode is a homogeneous state and hence translationally invariant, the phase of the corresponding envelope function decouples from the dynamics of remaining components (Matthews and Cox, 2000). Consequently, only the real component  $B(x, t)$  of this envelope function needs to be considered. The evolution equations for the envelope functions are often referred to as the Landau–Ginzburg equations or the Newell–Whitehead–Segel equations (Newell and Whitehead, 1969; Segel, 1969).

*Striped patterns:* Require an expansion that contains one critical  $\mathbf{q}$ -vector and the  $\mathbf{q} = 0$  mode. The spatio-temporal dynamics of the corresponding envelope function  $A(x, t)$  and  $B(x, t)$  are

$$\partial_t A = rA + \left( \partial_x + \frac{1}{2iq_c} \partial_{y^2} \right)^2 A - g|A|^2 A - h_2 BA, \quad (29)$$

$$\partial_t B = \nabla^2 B + \frac{h_2}{q_c^2} \nabla^2 |A|^2, \quad (30)$$

where  $g = -2h_2^2/Q^2 + (3h_3/2)$ .

*Square patterns:* Require an expansion with two orthogonal critical  $\mathbf{q}$ -vectors and the  $\mathbf{q} = 0$  mode. The spatio-temporal dynamics of the two complex envelope functions  $A_1(x, t)$  and  $A_2(x, t)$  and that of the real envelope function  $B(x, t)$  are

$$\partial_t A_i = rA_i + (\mathbf{n}_i \cdot \nabla)^2 A_i - g|A_i|^2 A_i - g_s |A_{3-i}|^2 A_i - h_2 BA_i, \quad i, j = 1, 2, \quad (31)$$

$$\partial_t B = \nabla^2 B + \frac{h_2}{q_c^2} \nabla^2 (|A_1|^2 + |A_2|^2), \quad (32)$$

where  $g$  is the same as above,  $g_s = 3h_3$  and  $\mathbf{n}_i$  is the unit vector along the direction of  $\mathbf{q}_i$  (see Appendix B).

*Hexagonal patterns:* Require an expansion in three critical  $\mathbf{q}$ -vectors oriented at  $120^\circ$  with each other. The spatio-temporal dynamics of the envelope functions  $A_1(x, t)$ ,  $A_2(x, t)$ ,

$A_3(x, t)$  and  $B(x, t)$  are given by

$$\partial_t A_i = r A_i + (\mathbf{n}_i \cdot \nabla)^2 A_i - h_2 A_{i+1}^* A_{i-1}^* - \frac{2ih_2}{q_c} [A_{i+1}^* (\mathbf{n}_{i-1} \cdot \nabla) A_{i-1}^* + A_{i-1}^* (\mathbf{n}_{i+1} \cdot \nabla) A_{i+1}^*] - g |A_i|^2 A_i - g_h (|A_{i+1}|^2 + |A_{i-1}|^2) A_i - h_2 B A_i \quad (i = 1, 2, 3), \tag{33}$$

$$\partial_t B = \nabla^2 B + \frac{h_2}{q_c^2} \nabla^2 (|A_1|^2 + |A_2|^2 + |A_3|^2), \tag{34}$$

where  $g$  is the same as before,  $g_h = 3h_3 - (2h_2^2/(2 - \sqrt{3})Q^2)$  and  $\mathbf{n}_i, \mathbf{n}_{i+1}, \mathbf{n}_{i-1}$  are unit vectors along the directions of wave-vector  $\mathbf{q}_i, \mathbf{q}_{i+1}$  and  $\mathbf{q}_{i-1}$ , respectively (Appendix B). In these expressions  $i - 1$  and  $i + 1$  are used as a shorthand notation  $1 + i(\text{mod } 3)$  and  $1 + (i + 1)(\text{mod } 3)$ , respectively.

We can use the Newell–Whitehead–Segel equations to determine, theoretically, the stability domains for striped, square and hexagonal arrays, and to determine all allowed structures at a given fractional coverage  $C_0$  of the monolayer. Since several prefactors of the Suo–Lu equations depend on  $C_0$  (see Eqs. (12) and (26)–(28)), the application of multiple scales analysis will be more complex than that for typical cases. For parameters used by [Suo and Lu \(2000, 2001\)](#) the coefficient  $g$  is negative when the uniform state destabilizes. This corresponds to a subcritical bifurcation. Consequently, a quintic term must be present to quench the growth of the envelope functions. Rather than pursuing a full description of this system, which requires an expansion to fifth order in  $\varepsilon$  (a very laborious process), we illustrate multiple scales analysis of the Suo–Lu model with  $Q = 1.6$  and  $\Omega = 1.6$ . Then,  $g$  is positive in the entire range of concentrations beyond the onset of the instability, and hence  $r > 0$ . The dependence of the coefficients of the Newell–Whitehead–Segel equations for the Suo–Lu model as a function of  $C_0$  are shown in [Fig. 4](#).

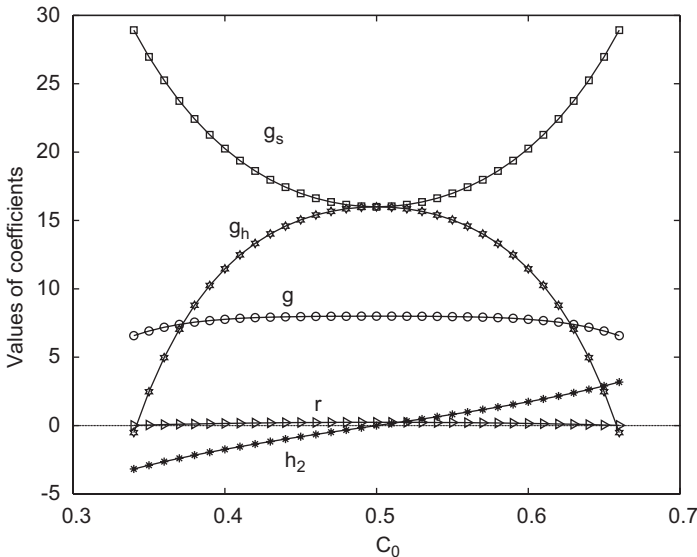


Fig. 4. The values of the coefficients of the Suo–Lu equations at mean concentrations in the range  $C_0 \in [0.33, 0.67]$ . The other (fixed) control parameters are  $Q = 1.6$ , and  $\Omega = 1.6$ . The relative ordering of these coefficients determine the stability of patterns at a given set of parameters.

It should be noted that for a system with  $\Omega = 1.6$ , the function of free energy  $g(C)$  (Suo and Lu, 2000, p. 339) is convex and hence, by itself, does not create conditions for phase separation. However, phase separation is not the only determining factor for pattern formation. Rather, the ordering of the monolayer is determined by minimizing the sum of free energy, phase boundary energy, and elastic energy (Suo and Lu, 2000). In the system we considered,  $r$  is positive when  $C_0 \in [0.34, 0.66]$  and negative otherwise. Although its magnitude is much smaller than those of other coefficients, only a system with a positive  $r$  can break the symmetry of the uniform state to create self-assembled structures. It should be noted though, that specially prepared initial states with finite amplitude can be stable to small perturbations (see below).

The coefficient  $h_2$ , which couples the envelope functions  $B(x, t)$  and  $A_i(x, t)$ , is negative when  $C_0 < 0.5$  and positive when  $C_0 > 0.5$ . As discussed below, it is related to the stability of various planforms and the appearance of low- $C_0$  and high- $C_0$  droplets. Square patterns are unstable for all fractional coverages of the monolayer because  $g_s > g$ .  $g_h$  is less than  $g$  close to the onset of instability, but larger than  $g$  when  $C_0$  is close to 0.5. This relationship determines the stability of striped arrays against the oblique-roll instability (see the next section).

## 6. Instabilities of striped patterns

Instabilities of striped arrays, such as the Eckhaus and zigzag instabilities, have been extensively studied over the past several decades (e.g., Cross and Hohenberg, 1993). More recent studies have investigated them in conservative systems, i.e., in the presence of a marginal mode at  $\mathbf{q} = 0$  (Matthews and Cox, 2000; Golovin et al., 1994, 1997). For models studied earlier, it was found that the inclusion of the marginal mode changes the stability diagram significantly. We analyze the Newell–Whitehead–Segel equations for the Suo–Lu model using the magnitude and phase of the envelope functions (Hoyle, 1998). We calculate, theoretically, instabilities of striped, square and hexagonal patterns, and compare stability boundaries with those on numerical integrations of the Suo–Lu model.

### 6.1. Perturbation analysis

The steady state striped solution of Eqs. (29)–(30) is

$$A = R_0 e^{ikx}, \quad B = 0, \tag{35}$$

where  $k = q - q_c$ , and  $R_0^2 = (r - k^2)/g$ . Perturbations of amplitude and phase are written as  $A = R_0(1 + R)e^{i(kx+\phi)}$  and  $B = b$ , where  $|R| \ll 1$ ,  $|\phi| \ll 1$ , and  $|b| \ll 1$  (Hoyle, 1998). They evolve according to

$$R_t = -2gR_0^2 R - 2k\phi_x + R_{xx} + \phi_{xyy} + kR_{yy} - (1/4)R_{yyy} - h_2 b, \tag{36}$$

$$b_t = b_{xx} + b_{yy} + \frac{2R_0^2 h_2}{q_c^2} (R_{xx} + R_{yy}), \tag{37}$$

$$\phi_t = 2kR_x + \phi_{xx} - R_{xyy} + k\phi_{yy} - (1/4)\phi_{yyy}. \tag{38}$$

We write  $R = \hat{R}e^{\sigma t + imx + ily}$ ,  $b = \hat{b}e^{\sigma t + imx + ily}$  with  $|m| \ll 1, |l| \ll 1$ , and find growth rate eigenvalues

$$\sigma_1 = -gR_0^2 - m^2 - \sqrt{(gR_0^2)^2 + \frac{2R_0^2 h_2^2 m^2}{q_c^2}}, \tag{39}$$

$$\sigma_2 = -gR_0^2 - m^2 + \sqrt{(gR_0^2)^2 + \frac{2R_0^2 h_2^2 m^2}{q_c^2}}, \tag{40}$$

for perturbations in the  $x$  direction ( $l = 0$ ). Corresponding equations for perturbations in the  $y$ -direction ( $m = 0$ ) can be derived.

The first eigenvalue is always negative and hence any perturbation will decay in time. However, the second may be positive. If  $gR_0^2 = O(1)$  (which is always true for the Suo–Lu system) the second growth rate can be approximated as

$$\sigma_2 \approx -m^2 \left( 1 - \frac{h_2^2}{gq_c^2} \right). \tag{41}$$

We find that  $h_2^2/gq_c^2 < 1$  when the mean concentration  $C_0 \in [0.38, 0.62]$ , which contains parameters for the stripe-hexagon transition (see below). Therefore, the coupling of the large-scale mode will not be relevant for the transition. In other words, the stability boundaries of the Suo–Lu system will not be altered significantly by inclusion of the  $\mathbf{q} = 0$  mode. All conclusions stated above have been verified using numerical integrations of the model.

Next we consider the instability caused by the phase perturbation. Taking  $\phi = \hat{\phi}e^{\sigma t + imx + ily}$ , with  $|m| \ll 1, |l| \ll 1$  and assuming that the large-scale mode is stable, the growth rate for the phase  $\hat{\phi}$  (Hoyle, 1998) is given by

$$\sigma_3 = -m^2 \left( 1 - \frac{2k^2}{R_0^2} \right) - kl^2 - \frac{2km^2 l^2}{R_0^2} - \frac{l^4}{4} + O(m^6). \tag{42}$$

For a perturbation in the  $x$  direction ( $l = 0$ ), the well-known Eckhaus instability results when  $r < 3k^2$ . For a perturbation in the  $y$  direction ( $m = 0$ ),  $\sigma_3$  is positive when  $k < 0$  and  $|l|$  is small enough ( $l^2 < -4k$ ). This is the zigzag instability. The presence of both instabilities have been confirmed by numerical integrations of the Suo–Lu model (see below).

Cross-roll and oblique-roll instabilities can also be studied (Hoyle, 1998). They are caused by perturbation of a roll growing at an angle to the original stripes, i.e., they are instabilities of amplitude. A straightforward way to investigate these effects is to adapt amplitude equations for square and hexagonal patterns, respectively, in performing the perturbation analysis. We use a set of coupled equations:

$$\partial_t A_1 = rA_1 + \left( \partial_{x_1} + \frac{1}{2iq_c} \partial_{y_1^2} \right)^2 A_1 - g|A_1|^2 A_1 - g_c|A_2|^2 A_1, \tag{43}$$

$$\partial_t A_2 = rA_2 + \left( \partial_{x_2} + \frac{1}{2iq_c} \partial_{y_2^2} \right)^2 A_2 - g|A_2|^2 A_2 - g_c|A_1|^2 A_2, \tag{44}$$

where  $g_c = g_s$  (see Eq. (31)) if the angle between the two sets of stripes is  $\pi/2$ , and  $g_c = g_h$  (defined in Eq. (33)) if the angle is  $\pi/3$ . Initially,  $A_1 = R_0 e^{ikx_1}$  with  $R_0^2 = (r - k^2)/g$ . For a

small perturbation  $A_2 = a_2 e^{ipx_2}$  with  $|a_2| \ll 1$ , one finds

$$\partial_t a_2 = \left[ r - p^2 - \frac{g_c}{g}(r - k^2) \right] a_2. \tag{45}$$

The fastest growing mode has  $p = 0$ , and it is unstable when  $r(1 - (g_c/g)) > -(g_c/g)k^2$ . For the perturbation from a perpendicular direction,  $g_c$  is always larger than  $g$  (see Fig. 4), and stripes are unstable for  $k^2 > r(1 - (g/g_c))$ . The stability boundaries of stripes to these perturbations is found to be wider than that of the Eckhaus and zigzag instabilities. The oblique-roll instability is different since, in the range of concentration we consider,  $g_c$  can be either larger or smaller than  $g$  (see Fig. 4). If  $g_c < g$  (i.e.,  $C_0 < 0.37$ ), one finds  $r - (g_c/g)(r - k^2)$  is always positive, and hence stripes are always unstable to the perturbation of an angle of  $\pi/3$ . In the range of concentration where  $g_c > g$ , the condition for instability is still  $r(1 - (g_c/g)) > -(g_c/g)k^2$ . Its boundary is narrower than that of the Eckhaus instability if and only if  $g_c/g < \frac{2}{3}$ .

In summary, striped patterns are stable in a region bounded by three curves corresponding to Eckhaus ( $k > \sqrt{r/3}$ ), zigzag ( $k < 0$ ), and oblique-roll ( $k > \sqrt{r(1 - g/g_c)}$ ) instabilities. It is also bounded above by the peak value  $\Omega + Q^2/4 - 2$  of  $r$ . The schematic diagram for the stability region of the striped patterns for the Suo–Lu model is shown in Fig. 5.

6.2. Numerical integration of stability domains

Next, we obtain stability maps for striped arrays using numerical integrations of Eq. (4). In particular, we search for the range of wave-vectors for which they are stable to small perturbations. For each wave-vector  $\mathbf{q}$ , we determine stability or instability by determining whether the initial state evolves to a striped array of wave-vector  $\mathbf{q}$  (stable) or to a different structure (unstable).

Most of our studies are conducted for critical wavenumber  $q_c = 0.8$ . Due to symmetry of textures about  $C_0 = 0.5$ , only the range  $C_0 \in [0.34, 0.50]$  is analyzed. The zigzag instability is seen when  $q < q_c$ . Fig. 6(a) shows some snapshots of the evolution with  $C_0 = 0.5$  and  $q = 0.7$ . The modulations normal to the initial striped array become noticeable at  $t \sim 446$ .

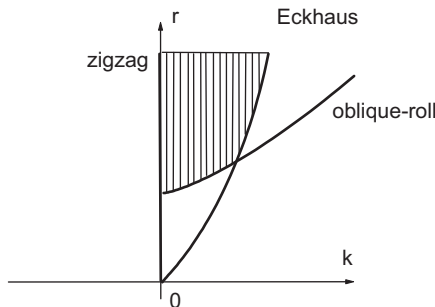


Fig. 5. Stability boundaries of striped patterns for the Suo–Lu model. The hatched region, where striped arrays are stable to small perturbations, is bounded on the left by the zigzag instability and on the right by the Eckhaus and oblique-roll instabilities. The horizontal line on top is the peak value of  $r = \Omega + Q^2/4 - 2$  (see Eq. (12)).

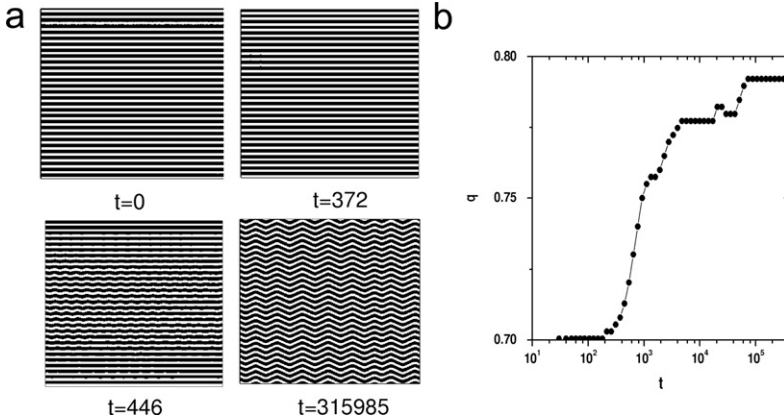


Fig. 6. (a) Snapshots of the spatiotemporal dynamics from an initially striped state ( $C_0 = 0.5, R = 0.01, q = 0.7$ ) under Eq. (4). The parameters used for the integration are  $Q = 1.6, \Omega = 1.6$ . The zigzag instability is clearly seen after  $t \sim 446$ . (b) The variation of the mean wavenumber, calculated using disorder function methods, during the evolution.

The final state is a regular wavy pattern with wavenumber close to  $q_c$ . We can use the recently developed *disorder function* analysis (Gunaratne et al., 1999) to find how the mean wavenumber changes during evolution of the texture. It is shown in Fig. 6(b). Similar behavior is observed for all  $q$  within  $[0.65, 0.75]$ . Initial states with  $q < 0.65$  lose their symmetry immediately and evolve to disordered labyrinthine patterns, which are similar to asymptotic structures generated from random initial states.

Striped initial states with small amplitude destabilize to hexagonal patterns when  $C_0 < 0.41$ . For  $C_0 \in (0.41, 0.47)$  both striped and hexagonal arrays can be stable to small perturbations; i.e., there is bistability. We also note that the asymptotic wavenumbers in systems with  $C_0 \approx 0.41$  can fall below the zigzag boundary  $q_c = 0.8$ . As an example, if a system at  $C_0 = 0.41$  is initiated with a striped state of  $q = 0.75$ , it appears to evolve to a final striped state with the same wave-vector. At this point, we are unable to explain this phenomenon. Finally, the boundary of the stability domain for  $C_0 < 0.47$  is consistent with that for the oblique roll instability. Fig. 7 compares the theoretical and numerical stability maps.

### 7. Instabilities of square patterns

A perfect square array of slightly off-critical wavenumber  $q = q_c + k$  is given by  $A_1 = R_0 e^{ikx}, A_2 = R_0 e^{iky}$ , and  $B = 0$ . According to the Newell–Whitehead–Segel equations (31)–(32)

$$R_0^2 = \frac{r - k^2}{g + g_s}. \tag{46}$$

Once again, we consider perturbations in the forms  $A_1 = R_0(1 + a_1)e^{ikx + \phi}, A_2 = R_0(1 + a_2)e^{iky + \psi}, B = b$ , where  $|a_1|, |a_2|, |\phi|, |\psi|, |b| \ll 1$ . They are found to evolve

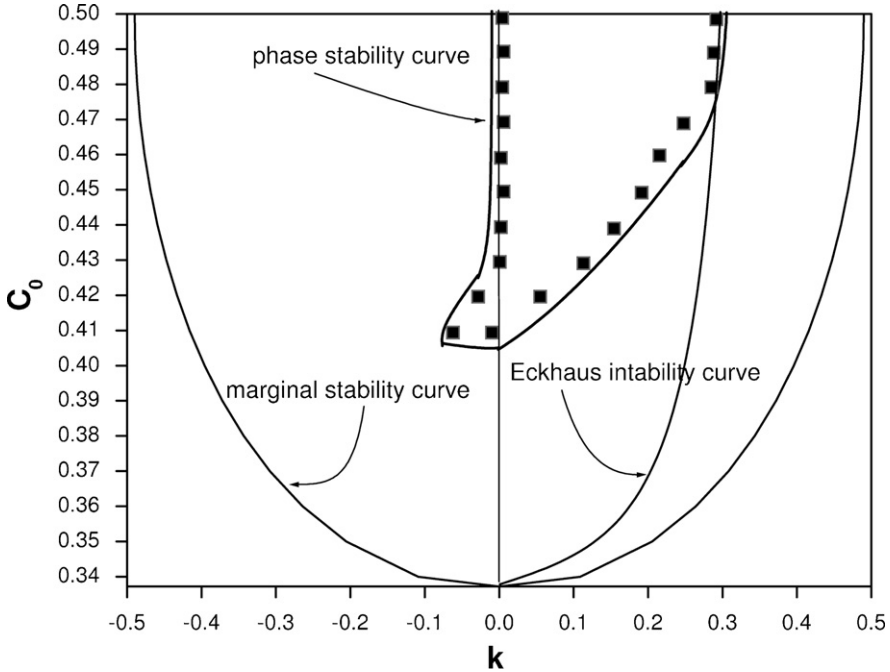


Fig. 7. Numerically computed stability boundaries for striped solutions of Eq. (4), with parameters  $Q = 1.6, \Omega = 1.6$ . Filled squares show the minimum and maximum wavenumbers of striped arrays that are stable at a given value of  $C_0$ . These results should be compared with theoretical calculations, shown in Fig. 5.

according to

$$\partial_t a_1 = -2gR_0^2 a_1 - 2g_s R_0^2 a_2 - \partial_x^2 a_1 - 2k \partial_x \phi - h_2 b, \tag{47}$$

$$\partial_t a_2 = -2gR_0^2 a_2 - 2g_s R_0^2 a_1 - \partial_y^2 a_2 - 2k \partial_y \psi - h_2 b, \tag{48}$$

$$\partial_t b = (\partial_x^2 + \partial_y^2) b + \frac{2R_0^2 h_2}{q_c^2} ((\partial_x^2 + \partial_y^2)(a_1 + a_2)), \tag{49}$$

$$\partial_t \phi = 2k \partial_x a_1 + \partial_x^2 \phi, \tag{50}$$

$$\partial_t \psi = 2k \partial_y a_2 + \partial_y^2 \psi. \tag{51}$$

Consider amplitude perturbations with fixed phases  $\phi$  and  $\psi$ . Let  $a_1 = \hat{a}_1 e^{\sigma t + imx + i ly}$ ,  $a_2 = \hat{a}_2 e^{\sigma t + imx + i ly}$ ,  $b = \hat{b} e^{\sigma t + imx + i ly}$ , with  $|m| \ll 1, |l| \ll 1$ . The growth rates of eigenvalues for the amplitude modes  $(\hat{a}_1 + \hat{a}_2)$  and  $(\hat{a}_1 - \hat{a}_2)$  are

$$\sigma_1 = -2(g + g_s)R_0^2 + O(m^2, l^2), \tag{52}$$

$$\sigma_2 = -2(g - g_s)R_0^2 + O(m^2, l^2), \tag{53}$$

respectively (Hoyle, 1998). Since  $g_s > g$  for all  $C_0$ , the second mode is always unstable to amplitude perturbation. This conclusion has been confirmed by numerical integration of the Suo–Lu model. Any initially square array destabilizes to either a hexagonal or a striped pattern depending on the initial conditions and  $C_0$ .

## 8. Instabilities of hexagonal patterns

Many studies have been performed to investigate the formation and destabilization of hexagonal patterns (Palm, 1960; Busse, 1967). We first follow the analysis presented by Hoyle (1998) to discuss characteristics of hexagonal arrays in the absence of a conserved quantity, and subsequently consider effects of the  $\mathbf{q} = 0$  mode.

### 8.1. Hexagonal states

Hexagonal patterns observed in both A-rich and B-rich substrates can be analyzed using the Newell–Whitehead–Segel equations (33). The envelope functions for a steady hexagonal pattern at a slightly off-critical wavenumber  $q = q_c + |\mathbf{k}|$  can be written as

$$A_i = R_0 e^{i\mathbf{k}_i \cdot \mathbf{x}} \quad \text{with} \quad \mathbf{k}_1 = k \hat{\mathbf{x}}, \quad \mathbf{k}_2 = k \left( -\frac{1}{2} \hat{\mathbf{x}} + \frac{\sqrt{3}}{2} \hat{\mathbf{y}} \right), \quad \mathbf{k}_3 = k \left( -\frac{1}{2} \hat{\mathbf{x}} - \frac{\sqrt{3}}{2} \hat{\mathbf{y}} \right), \quad (54)$$

Small perturbations in amplitude  $(1 + a_i)$  and phase  $\phi_i$ , evolve according to

$$\begin{aligned} \partial_t a_1 = & (r - k^2) a_1 - \left[ h_2 R_0 (a_2 + a_3) + \frac{2h_2 R_0}{q_c} (k(a_2 + a_3) + \partial_{x_2} \phi_2 + \partial_{x_3} \phi_3) \right] \cos \Phi \\ & + \frac{2h_2 R_0}{q_c} (\partial_{x_2} a_2 + \partial_{x_3} a_3) \sin \Phi - 3g R_0^2 a_1 - 2g_{II} R_0^2 (a_1 + a_2 + a_3) \\ & - 2k \partial_{x_1} \phi_1 + \partial_{x_1}^2 a_1, \end{aligned} \quad (55)$$

$$\begin{aligned} \partial_t \phi_1 = & \left[ h_2 R_0 (a_2 + a_3) + \frac{2h_2 R_0}{q_c} (k(a_2 + a_3) + \partial_{x_2} \phi_2 + \partial_{x_3} \phi_3) \right] \sin \Phi \\ & + \frac{2h_2 R_0}{q_c} (\partial_{x_2} a_2 + \partial_{x_3} a_3) \cos \Phi + 2k \partial_{x_1} a_1 + \partial_{x_1}^2 \phi_1, \end{aligned} \quad (56)$$

and four additional equations obtained by permuting subscripts. Here  $\Phi = \sum_i \phi_i$ . In the absence of spatial modulation the total phase evolves according to

$$\Phi_t = 2h_2 R_0 (a_1 + a_2 + a_3) \sin \Phi. \quad (57)$$

Therefore, at the stable steady state,  $\Phi$  takes the values  $\pi$  or  $0$  according to the sign of  $h_2$  ( $h_2 < 0 \rightarrow \Phi = 0$ ;  $h_2 > 0 \rightarrow \Phi = \pi$ ). In systems with  $\Phi = 0$ , the center of each hexagonal cell has the highest magnitude, while in systems with  $\Phi = \pi$ , it has the lowest magnitude. In Rayleigh–Bénard convection, these are known as “*l*-hexagons” and “*g*-hexagons”, respectively (Palm, 1960). Thus, the description of spatio-temporal dynamics via the Newell–Whitehead–Segel equations is consistent with results of numerical simulations (compare Figs. 3 and 4).

### 8.2. Transition from the homogeneous solution to hexagons

The presence of a set of  $C_0$ 's where the Suo–Lu system supports both hexagons and the homogeneous solution can be demonstrated using the Newell–Whitehead–Segel Eq. (33)

with no  $\mathbf{q} = 0$  mode. It can be inferred from (55) that (Hoyle, 1998)

$$\partial_t(a_1 + a_2 + a_3) = -v(a_1 + a_2 + a_3), \tag{58}$$

$$\partial_t(a_i - a_j) = -2u(a_i - a_j), \quad i \neq j, \tag{59}$$

where

$$u = R_0^2(g - g_h) + |h_2| \left(1 + \frac{2k}{q_c}\right) R_0, \tag{60}$$

$$v = 2R_0^2(g + 2g_h) - |h_2| \left(1 + \frac{2k}{q_c}\right) R_0. \tag{61}$$

Notice that the hexagonal state is unstable when  $v < 0$  (since  $a_1 + a_2 + a_3$  grows) or when  $u < 0$  (since  $a_i - a_j$  grows). From Eq. (54) it is obvious that there are always two branches of steady hexagonal solutions,

$$R_0^+ = \frac{1}{2(g + 2g_h)} \left[ |h_2| \left(1 + \frac{2k}{q_c}\right) + \sqrt{h_2^2 \left(1 + \frac{2k}{q_c}\right)^2 + 4(g + 2g_h)(r - k^2)} \right], \tag{62}$$

and

$$R_0^- = \frac{1}{2(g + 2g_h)} \left[ |h_2| \left(1 + \frac{2k}{q_c}\right) - \sqrt{h_2^2 \left(1 + \frac{2k}{q_c}\right)^2 + 4(g + 2g_h)(r - k^2)} \right]. \tag{63}$$

Growth rates  $u$  and  $v$  of these two branches for  $C_0 \in [0.34, 0.66]$  are shown in Fig. 8.  $R_0^-$  is unstable in the entire range because  $v < 0$ . On the other hand,  $R_0^+$  is unstable when  $C_0 \in [0.47, 0.53]$ . Inclusion of spatial modulations alters the stability boundaries slightly.

The transition from the homogeneous solution to hexagonal states is a subcritical bifurcation, see Fig. 10. Hexagons with  $k = 0$  exist if  $h_2^2 + 4(g + 2g_h)r > 0$ . We find that  $g + 2g_h > 0$  if and only if  $C_0 > 0.33$ . Hence the condition for hexagons to exist is trivially satisfied for  $C_0 > 0.3$ . In general, it is found that this condition holds when  $C_0 > 0.30$ , and hence hexagonal arrays given by Eqs. (62) and (63) exist for  $C_0 > 0.30$ . Consequently, the

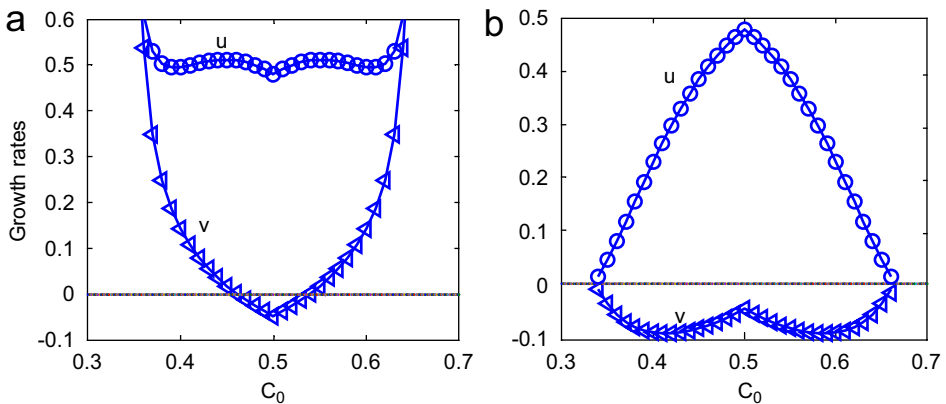


Fig. 8. The growth rates  $u$  and  $v$  when spatial modulations are ignored: branches with (a)  $R_0 = R_0^+$  and (b)  $R_0 = R_0^-$ . The hexagonal state is unstable if either  $u$  or  $v$  is negative.

bistable region where both the uniform solution and a hexagonal array can be stable is  $C_0 \in (0.30, 0.34)$ .

This assertion is confirmed by numerical integrations of the Suo–Lu equation. We find that initial hexagon states with sufficiently small amplitude (e.g., 0.01) gradually degrades to the homogeneous state. In contrast, for large initial amplitudes (e.g.,  $R_i = 0.1$ ) the system evolves to a steady hexagonal array. In addition, numerical integration validates theoretical estimates for the domain of bistability.

### 8.3. Transition from hexagonal to striped arrays

Next we analyze the stripe-hexagon transition. Numerically, we find by using the Suo–Lu model with  $Q = 1.6$ ,  $\Omega = 1.6$  and  $C_0 \in [0.46, 0.54]$ , that an initially prepared hexagonal state of any wavenumber destabilizes to stripes; systems with  $C_0$  outside of this range can support suitably prepared hexagonal and striped states whose wavenumbers are sufficiently close to  $q_c$ .

We can use the Newell–Whitehead–Segel equations to analyze the transition theoretically. A stripe-like perturbation of the hexagonal state can be expressed as  $A_1 = R_0(1 + a_1)e^{ik_1 \cdot x + \phi_1}$ ,  $A_2 = a_2 e^{ik_2 \cdot x + \phi_2}$ ,  $A_3 = a_3 e^{ik_3 \cdot x + \phi_3}$ , where  $|\mathbf{k}| = q - q_c$  and  $R_0^2 = (r - k^2)/g$ ; they evolve according to

$$\partial_t a_1 = -2gR_0^2 a_1, \quad (64)$$

$$\partial_t a_2 = R_0^2(g - g_h)a_2 + |h_2|R_0 a_3, \quad (65)$$

$$\partial_t a_3 = R_0^2(g - g_h)a_3 + |h_2|R_0 a_2, \quad (66)$$

The growth rates are  $-2gR_0^2$ ,  $R_0^2(g - g_h) \pm |h_2|R_0$ . At the critical wavenumber ( $k = 0$ ), the largest growth rate is positive for  $C_0 < 0.44$  (and symmetrically at  $C_0 > 0.56$ ) (see Fig. 9). Consequently, the range of concentrations for stable stripes is narrower than that due to the oblique-roll instability (which is  $C_0 \in [0.37, 0.63]$ ). When spatial modulations are allowed and  $k \neq 0$ , it is seen that the stability domain increases and is closer to that evaluated from numerical integration (i.e.,  $C_0 \in [0.41, 0.59]$ , see Fig. 10). Stability domains for striped and hexagonal patterns are summarized in Fig. 10.

### 8.4. Effect of the $\mathbf{q} = 0$ mode on the hexagonal state

Coupling of the large scale mode to hexagonal patterns can be analyzed in a manner similar to that for striped arrays. If phase variables are kept constant, hexagonal amplitudes multiplied by  $(1 + a_i)$ , and a large scale mode of magnitude  $b$  is introduced, the spatio-temporal dynamics reduces to

$$\begin{aligned} \partial_t(a_1 + a_2 + a_3) &= -v(a_1 + a_2 + a_3) + \sum_{i=1}^3 \partial_{x_i}^2 a_i - 3h_2 b, \\ \partial_t b &= \nabla^2 b + \frac{2R_0^2 h_2}{q_c^2} \nabla^2 \sum_i a_i, \quad i = 1, 2, 3. \end{aligned} \quad (67)$$

Because,  $\Phi = \sum \phi_i$  takes a fixed value in the absence of spatial modulations, the fastest growing modes are those along the directions of the hexagonal modes (Hoyle, 1998), and the perturbations are  $a_i = \hat{a}_i e^{i\hat{L}x_i}$ , and  $b = \hat{b} e^{i\hat{L}\tilde{x}}$  where  $\tilde{x}$  can be an arbitrary direction. It is

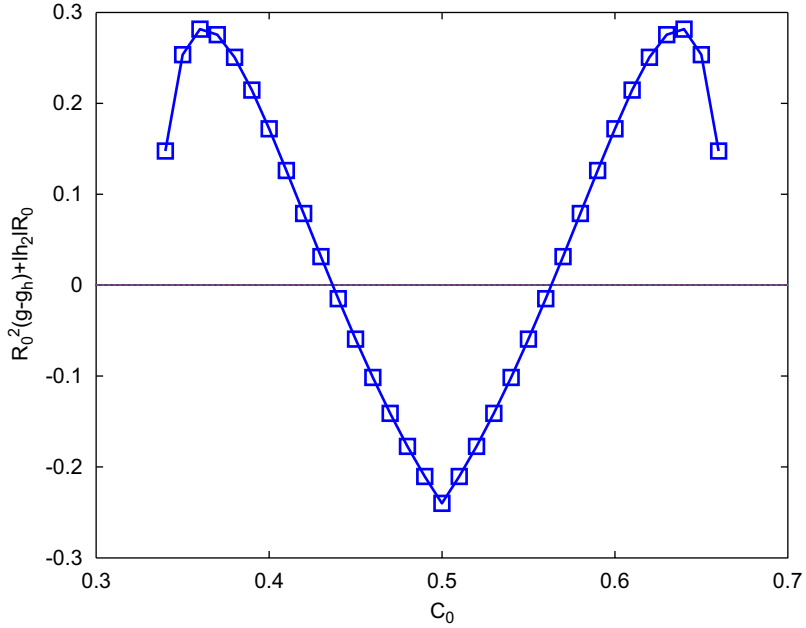


Fig. 9. The growth rate of the most dangerous mode for the perturbations to stripes, obtained using Eq. (33). The parameters used are  $Q = 1.6, \Omega = 1.6,$  and  $k = 0.$

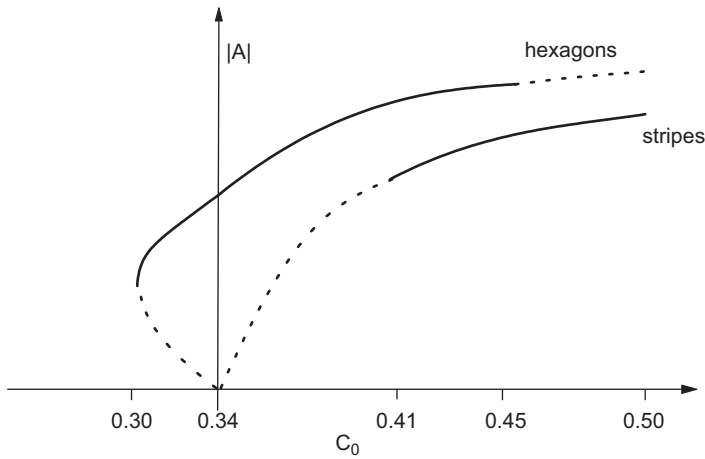


Fig. 10. Bifurcation diagram for the striped and hexagonal patterns in the Suo–Lu model. Stable and unstable solution branches are indicated by solid and dotted lines, respectively.

found that the growth rates  $\sigma$  satisfies

$$(v + l^2 + \sigma)(l^2 + \sigma) - \frac{6h_2^2 R_0^2 l^2}{q_c^2} = 0, \tag{68}$$

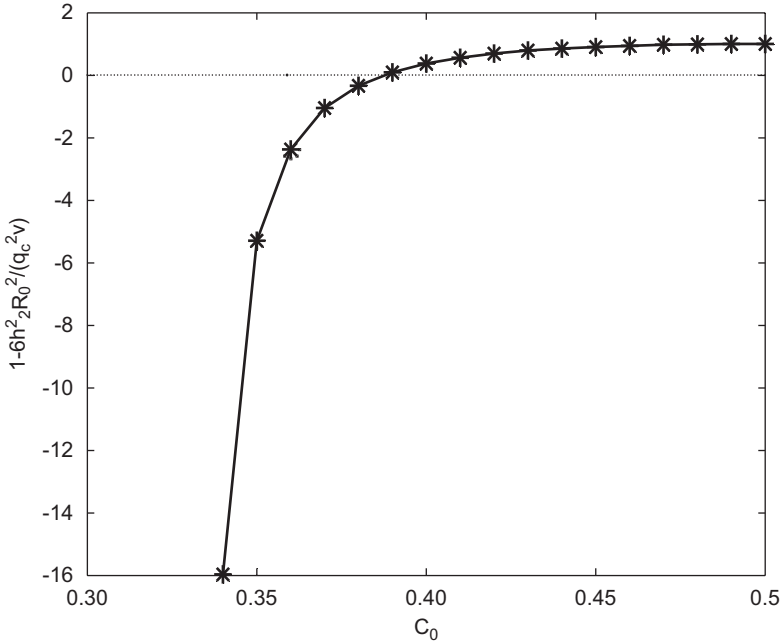


Fig. 11. The values of  $1 - (6h_2^2 R_0^2 / q_c^2 v)$  in the systems where  $C_0 \in [0.34, 0.50]$ ,  $Q = 1.6$ , and  $\Omega = 1.6$ .

with  $v$  defined in Eq. (61). Since the most dangerous disturbance occurs in the limit  $l \rightarrow 0$ , the growth rate of the large scale mode can be approximated as

$$\sigma = -l^2 \left( 1 - \frac{6h_2^2 R_0^2}{q_c^2 v} \right), \tag{69}$$

which is positive if  $1 - (6h_2^2 R_0^2 / q_c^2 v) < 0$ . The values of  $1 - (6h_2^2 R_0^2 / q_c^2 v)$  for  $C_0 \in [0.34, 0.50]$  are plotted in Fig. 11. According to this analysis, perfect hexagonal patterns will lose stability when  $C_0 \in [0.34, 0.38]$ . The instability can develop either through a supercritical or a saddle-node bifurcation, with amplitudes suppressed in some regions and enhanced in others (Matthews and Cox, 2000). In one dimensional systems it was found that the instability can only be observed in sufficiently large domains and with sufficiently small driving parameters (Matthews and Cox, 2000). For the two dimensional Suo–Lu model system, we have not found such modulated structures, even for very large systems. It is possible that the large amplitude of the hexagonal state (due to the subcritical transition) plays a role in this disagreement. Further investigation is needed to address this issue.

### 9. Concluding discussions

We conducted a theoretical analysis of nano-scale self-assembly by using techniques from pattern formation (Cross and Hohenberg, 1993) to study a paradigmatic model (1) which describes spatio-temporal dynamics of the (coarse-grained) concentration field  $C(x, y)$  of epilayer atoms on a substrate. The model system which incorporates phase separation, coarsening, and refining exhibits many features observed in experiments on

vapor deposition (Pohl et al., 1999; Plass et al., 2001). The linear and nonlinear stability analyses reported here were conducted on Eq. (1) with the parameters  $Q$  and  $\Omega$ , each fixed at 1.6, and using the mean coverage  $C_0 = \langle C(x, y) \rangle$  as the control parameter.

There is a symmetry in self-assembly between the deposit-rich ( $C_0 > \frac{1}{2}$ ) and the deposit-poor ( $C_0 < \frac{1}{2}$ ) phases of the monolayer; consequently, we limit our studies to the range  $C_0 \in (0, \frac{1}{2})$ . Due to conservation of the total number of particles on the monolayer, Eq. (1) has a marginal mode at zero wave-vector. The homogeneous solution is the only stable state for low concentrations of the deposition. As  $C_0$  is increased, it is destabilized by Fourier modes with non-zero wave-vectors. Nonlinear terms in Eq. (1) determine the type of structures that can result beyond this stage.

The rest of our analysis focuses on periodic textures that cover the surface, namely, striped, square, and hexagonal arrays. Their existence and properties are calculated using nonlinear stability analysis. The analysis requires a real envelope function associated with the zero wave-vector mode and one, two or three complex envelope functions for striped, square, and hexagonal arrays, respectively. These calculations were done using the spatio-temporal dynamics for the magnitude and phase of these envelope functions.

The homogeneous solution was shown to destabilize at  $C_0 \approx 0.34$  via a subcritical (or backward) bifurcation to a hexagonal array. Suitably prepared steady homogeneous solutions and hexagonal arrays can be found within the bistable region  $C_0 \in [0.30, 0.34]$ . As  $C_0$  is increased further, the hexagonal state destabilizes to a striped array at  $C_0 = 0.47$  via a second subcritical bifurcation. Depending on the initial structure, both hexagonal and striped arrays can stabilize for  $C_0 \in (0.41, 0.47)$ . These assertions were validated in numerical integrations of Eq. (1). Within  $C_0 \in (0.41, 0.47)$  it is possible to form (apparently) steady complex structures that have locally hexagonal and locally striped domains. Similarly, except for specially prepared initial systems, patterns seen for  $C_0 > 0.47$  are labyrinthine, consisting of multiple patches of locally striped domains.

We calculated the stability map for striped arrays by considering perturbations that give Eckhaus, zigzag, and cross-roll instabilities. Numerical analysis validated these theoretical assertions, except in a very small set of parameters where the predicted zigzag instability was not observed. It is possible that the time scale for the instability to set in is longer than the time interval for which Eq. (1) was integrated. We also presented analogous calculations for the square and hexagonal arrays. One point worth noting is that, for the control parameters  $Q$  and  $\Omega$  that were used, square arrays are unstable in the entire range of coverages, destabilizing either to striped or hexagonal arrays.

Our analytical studies on the formation and stability of nanostructures can help address many issues that may be important in self-assembly. As an example, identifying systems that generate self-assembled square arrays is of interest in developing high-density magnetic storage. Can such states form in the Suo–Lu system for a suitable choice of system parameters? If not, can the system be modified in order for it to form self-assembled square arrays? Analyses presented in the paper, coupled with the thermodynamic models such as that introduced by Suo and Lu, can provide a theoretical framework for addressing such questions, and in general, for studying guided self-assembly of nanostructures.

The availability of a theoretical framework can also be used in an inverse approach to extract material properties of self-assembled nanostructures that may otherwise be hard to estimate. This suggestion is inspired by recently developed approaches to measure elastic moduli experimentally through wrinkling of thin films (e.g. Huang, 2005 and references therein). Here, a soft polymer substrate is deformed in tension along one direction. The

thin film is then deposited on the deformed substrate. Upon release of the substrate constraint, the film experiences compressive strains and is seen to form a wavy pattern. If no delamination takes place, the material is isotropic, and it remains linear and elastic, it can be shown that the buckling wavelength is related to the film thickness, as well as the elastic moduli and Poisson ratio of the film and substrate (Huang, 2005). The wavelength of a 30 nm thick metallic film on a polymer substrate ( $\sim 1000 : 1$  ratio in elastic moduli) is  $\sim 1 \mu\text{m}$  and is thus easily measured using optical microscopy. Consequently, it is possible to deduce (say) the elastic modulus of the film. In an exact analogy with the wrinkling based approach, one may take advantage of the numerous self-assembled patterns to find elusive properties such as surface stress or energy cost of concentration gradients ( $h_0$  in Eq. (1)) through the use of theoretical analysis on models of monolayer growth.

The work reported in this paper was conducted as a part of the doctoral research of Hu (2006). The authors would like to acknowledge the Texas Learning and Computation Center for usage of computers for the project. They would also like to thank Professor Wei Lu for encouraging comments. This research was partially supported by the Welch Foundation through grant E-0608 (SH and DJK), the Office of Naval Research Young Investigator Award N000140510662 (PS), the National Science Foundation through grant DMS-0607345 (GHG), and the Texas Center for Superconductivity (GN, FH and GHG).

#### Appendix A. Fourier transform of $I_0$ in the Suo–Lu equation

The surface strain in Eq. (4) has the form

$$I_0 = \iint \frac{(x - \xi_1) \left( \frac{\partial C}{\partial \xi_1} \right) + (y - \xi_2) \left( \frac{\partial C}{\partial \xi_2} \right)}{[(x - \xi_1)^2 + (y - \xi_2)^2]^{3/2}} d\xi_1 d\xi_2. \quad (70)$$

Its form in Fourier space can be obtained by transforming the boundary conditions and solving the elasticity problem in reciprocal space (Lu and Suo, 2002).

Writing  $I_0$  as  $I_a + I_b$ , with

$$I_a = \iint \frac{(x - \xi_1) \frac{\partial C}{\partial \xi_1}}{[(x - \xi_1)^2 + (y - \xi_2)^2]^{3/2}} d\xi_1 d\xi_2, \quad (71)$$

and

$$I_b = \iint \frac{(y - \xi_2) \frac{\partial C}{\partial \xi_2}}{[(x - \xi_1)^2 + (y - \xi_2)^2]^{3/2}} d\xi_1 d\xi_2, \quad (72)$$

and denoting  $\tilde{\rho} = [(x - \xi_1)^2 + (y - \xi_2)^2]^{1/2}$ , we have

$$\begin{aligned} \frac{\partial \tilde{\rho}^{-1}}{\partial \xi_1} &= -\tilde{\rho}^{-2} \frac{\partial \tilde{\rho}}{\partial \xi_1} \\ &= \frac{(x - \xi_1)}{\tilde{\rho}^3}. \end{aligned} \quad (73)$$

Hence

$$I_a = \iint \frac{\partial \hat{\rho}^{-1}}{\partial \xi_1} \frac{\partial C}{\partial \xi_1} d\xi_1 d\xi_2. \tag{74}$$

Eq. (74) is a convolution of  $\rho^{-1} = (x^2 + y^2)^{-1/2}$  and  $C(x, y)$ , i.e.,

$$I_a = -\frac{\partial \rho^{-1}}{\partial x} * \frac{\partial C}{\partial x}. \tag{75}$$

Similarly,

$$I_b = -\frac{\partial \rho^{-1}}{\partial y} * \frac{\partial C}{\partial y}. \tag{76}$$

Using the fact that the Fourier transform of a convolution is the product of the Fourier transform of the two functions, we have

$$\begin{aligned} \hat{I}_a &= -2\pi \frac{\widehat{\partial \rho^{-1}}}{\partial x} \widehat{\frac{\partial C}{\partial x}} \\ &= 2\pi q_x^2 \widehat{\rho^{-1}} \widehat{C}, \end{aligned} \tag{77}$$

and similarly for  $I_b$ . Therefore

$$\begin{aligned} \hat{I}_0 &= 2\pi(q_x^2 + q_y^2) \widehat{\rho^{-1}} \widehat{C} \\ &= 2\pi q^2 \widehat{\rho^{-1}} \widehat{C}. \end{aligned} \tag{78}$$

The Fourier transform of the radially symmetric function  $\rho^{-1}$  can be shown to be  $1/q$  using the Fourier–Bessel transform (Bracewell, 1999). Finally, we have

$$\hat{I}_0 = 2\pi q \widehat{C}. \tag{79}$$

## Appendix B. Derivation of amplitude equations for patterns

### B.1. Striped patterns

A locally striped pattern can be expanded as

$$C_1 = W_1 e^{i\mathbf{q}\cdot\mathbf{x}} + W_1^* e^{-i\mathbf{q}\cdot\mathbf{x}}, \tag{80}$$

where the envelope function  $W_1$  depends only upon slow variables.

1. At order of  $\varepsilon^1$ , we have

$$\nabla_0^2 (h_c + H_0) C_1 = 0, \tag{81}$$

where  $h_1 = h_c - 2r$ . As  $h_c = Q^2/2$ , the critical modes  $|\mathbf{q}| = q_c = Q/2$  are the eigenvectors with zero eigenvalue.

2. At order of  $\varepsilon^2$ ,

$$\partial_{\tau_1} C_1 = \nabla_0^2 [(h_c + H_0) C_2 + h_2 C_1^2 - 2r_1 C_1 + H_1 C_1] + 2\nabla_0 \nabla_1 (h_c + H_0) C_1. \tag{82}$$

Since  $H_1 C_1$  and  $(h_c + H_0) C_1$  vanish identically for the critical modes, and  $C_1^2$  has no contribution to the resonant term, the solvability condition requires (Newell and

Whitehead, 1969; Segel, 1969)

$$r_1 = 0, \quad \partial_{\tau_1} W_1 = 0. \quad (83)$$

As a result,  $\varepsilon \propto \sqrt{(h_c - h_1)/2}$ .

Since a large-scale mode ( $q = 0$ ) evolves on a long timescale, it is necessary to include it in the reduced dynamics. Following the examples of Matthews and Cox (2000) and Golovin et al. (1994), we consider a real amplitude  $U$  of large-scale at order of  $\varepsilon^2$ , write  $C_2$  as

$$C_2 = W_2 e^{i2\mathbf{q}\cdot\mathbf{x}} + \text{c.c.} + U. \quad (84)$$

It is easy to deduce from Eq. (82)

$$W_2 = -\frac{2h_2}{Q^2} W_1^2. \quad (85)$$

3. At order of  $\varepsilon^3$ , one obtains

$$\begin{aligned} \partial_{\tau_2} C_1 = & \nabla_0^2 [(h_c + H_0)C_3 - 2r_2 C_1 + 2h_2 C_1 C_2 + h_3 C_1^3 + H_1 C_2 - 2r_1 C_2 - 2\nabla_1^2 C_1] \\ & + 2\nabla_0 \nabla_1 [(h_c + H_0)C_2 - 2r_1 C_1 + h_2 C_1^2 + H_1 C_1] + \nabla_1^2 [(h_c + H_0)C_1]. \end{aligned} \quad (86)$$

The solvability condition requires

$$-\partial_{\tau_1} C_1 + \nabla_0^2 (2h_2 C_1 C_2 + h_3 C_1^3) - \nabla_0^2 (2r_2 C_1) - 2\nabla_0^2 \nabla_1^2 C_1 = 0. \quad (87)$$

The resonant terms in  $C_1 C_2$  are  $W_1^* W_2 + W_1 U$ , and that in  $C_1^3$  is  $3|W_1|^2 W_1$ . Since the slow scales of a striped structure in  $x$  and  $y$  direction scale differently,  $\nabla_0^2 \nabla_1^2$  need to be written as  $q_c^2 (\partial_X + (1/2iq_c)\partial_{Y^2})^2$  (Manneville, 1990, p. 327). Then the amplitude equation for  $W_1$  is

$$\partial_{\tau_2} W_1 = 2q_c^2 \left( r_2 W_1 + \left( \partial_X + \frac{1}{2iq_c} \partial_{Y^2} \right)^2 W_1 - g |W_1|^2 W_1 - h_2 U W_1 \right), \quad (88)$$

where  $g = (-2h_2^2/Q^2 + (3h_3/2))$ .

4. At order of  $\varepsilon^4$ , collecting the terms independent of the fast variables, one obtains:

$$\partial_{\tau_2} U = h_c \nabla_1^2 U + 2h_2 \nabla_1^2 |W_1|^2. \quad (89)$$

Unlike for critical modes (which have a chosen direction), dynamics of the envelope of the  $\mathbf{q} = 0$  mode should be isotropic. Thus, the spatio-temporal dynamics for the corresponding envelope function is

$$\partial_{\tau_2} U = h_c (\partial_{X^2} + \partial_{Y^2}) U + 2h_2 (\partial_{X^2} + \partial_{Y^2}) |W_1|^2. \quad (90)$$

Rewriting the equation in unscaled units

$$\begin{aligned} A(\mathbf{x}, t) = & \varepsilon W_1(X, Y, \tau_2); \quad B(\mathbf{x}, t) = \varepsilon^2 U(X, Y, \tau_2); \\ \varepsilon^2 r_2 = & r; \quad \varepsilon^2 \partial_{\tau_2} = \partial_t, \end{aligned}$$

and rescaling  $t \rightarrow t/2q_c^2$ , we obtain Eqs. (29)–(30).

### B.2. Square patterns

In this case, one has

$$C_1 = W_{11}e^{i\mathbf{q}_1 \cdot \mathbf{x}} + W_{12}e^{i\mathbf{q}_2 \cdot \mathbf{x}} + \text{c.c.}, \tag{91}$$

where  $\mathbf{q}_1$  and  $\mathbf{q}_2$  are normal to each other.

1. At order of  $\varepsilon$ , Eq. (81) is obtained. Therefore  $|\mathbf{q}_1| = |\mathbf{q}_2| = q_c$ .

2. At order of  $\varepsilon^2$ , one has Eq. (82). Since  $C_1^2$  still does not contribute to the resonant term, the amplitudes are independent of  $\tau_1$  and  $r_1 = 0$ . Writing

$$C_2 = W_{21}e^{i2\mathbf{q}_1 \cdot \mathbf{x}} + W_{22}e^{i2\mathbf{q}_2 \cdot \mathbf{x}} + \text{c.c.} + U, \tag{92}$$

we find that  $W_{2n} = -(2h_2/Q^2)W_{1n}^2 (n = 1, 2)$ .

3. At order of  $\varepsilon^3$ , Eq. (87) should be satisfied. The resonant terms in  $C_1C_2$  are the same as for the striped structure, but in  $C_1^3$ , they should include  $3|W_{11}|^2W_{11} + 6|W_{12}|^2W_{11}$ . Furthermore, for a square structure, the slow scales in  $x$  and  $y$  directions need not to be different (Pomeau and Manneville, 1980). Consequently, the equations for  $W_{11}$  and  $W_{12}$  are

$$\partial_{\tau_2} W_{11} = 2q_c^2(r_2W_{11} + (\mathbf{n}_1 \cdot \nabla_1)^2W_{11} - g|W_{11}|^2W_{11} - 3h_3|W_{12}|^2W_{11} - h_2UW_{11}), \tag{93}$$

$$\partial_{\tau_2} W_{12} = 2q_c^2(r_2W_{12} + (\mathbf{n}_2 \cdot \nabla_1)^2W_{12} - g|W_{12}|^2W_{12} - 3h_3|W_{11}|^2W_{12} - h_2UW_{12}), \tag{94}$$

where  $\mathbf{n}_1, \mathbf{n}_2$  are the unit vectors along the direction of  $\mathbf{q}_1$  and  $\mathbf{q}_2$ , and  $g = (-2h_2^2/Q^2 + (3h_3/2))$ .

4. At order of  $\varepsilon^4$ , collecting terms independent of rapid variables, one obtains

$$\partial_{\tau_2} U = h_c \nabla_1^2 U + 2h_2 \nabla_1^2 (|W_{11}|^2 + |W_{12}|^2). \tag{95}$$

Returning to the unscaled variables and rescaling  $t \rightarrow t/2q_c^2$ , we obtain Eqs. (31)–(32).

### B.3. Hexagonal patterns

Perturbed hexagonal states can be expanded as

$$C_1 = \sum_{n=1}^3 W_{1n}e^{i\mathbf{q}_n \cdot \mathbf{x}} + \text{c.c.}, \tag{96}$$

where the three vectors  $\mathbf{q}_1, \mathbf{q}_2$ , and  $\mathbf{q}_3$  bear angles  $2\pi/3$  with each other.

1. At order of  $\varepsilon$ , one has Eq. (81). Therefore  $|\mathbf{q}_n| = q_c$ .

2. At order of  $\varepsilon^2$ , one has Eq. (82). However,  $C_1^2$  has a term  $2W_{12}^*W_{13}^*$  that is resonant to  $W_{11}$ . Consequently, the solvability condition gives

$$\partial_{\tau_1} W_{11} = 2q_c^2(r_1W_{11} - h_2W_{12}^*W_{13}^*). \tag{97}$$

Since the coefficient of the quadratic term (i.e.,  $h_2$ ) is not small, we consider Eqs. (97) as explicit description of the dynamics of the system on the time scale  $t_1$ . A combination with the dynamics on scale  $t_2$  will give the complete description of the system. We can

write  $C_2$  as

$$C_2 = \sum_1 W_{2n} e^{i2\mathbf{q}_n \cdot \mathbf{x}} + \sum_2 V_{nm} e^{i(\mathbf{q}_n - \mathbf{q}_m) \cdot \mathbf{x}} + \text{c.c.} + U, \quad (98)$$

where  $\sum_1$  is the summation over  $n = 1, 2, 3$  and  $\sum_2$  is the summation over  $n, m = 1, 2, 3$  with  $n \neq m$ . Note that wavevectors of types  $(\mathbf{q}_n - \mathbf{q}_m)$  have been added to the *excited modes* at the second order, since the interactions of these modes with the basic lowest modes can also give resonant terms. These additional terms in a hexagonal basis were suggested by Gunaratne et al. (1994) and are needed for a complete description of instabilities of hexagonal arrays.

The relations between the amplitudes of the first harmonics and the second are

$$W_{2n} = -\frac{2h_2}{Q^2} W_{1n}^2, \quad (99)$$

$$V_{nm} = -\frac{2h_2}{(2 - \sqrt{3})Q^2} W_{1n} W_{1m}^*. \quad (100)$$

3. At order of  $\varepsilon^3$ , we once again have Eq. (87). The resonant terms to  $W_{11}$  in  $C_1 C_2$  are  $W_{11}^* W_{21} + W_{11} U + W_{12} V_{12} + W_{13} V_{13}$ , and in  $C_1^3$  are  $3|W_{11}|^2 W_{11} + 6(|W_{12}|^2 + |W_{13}|^2) W_{11}$ . Therefore the coefficients of the self-interacting terms are the same as those of the two planforms above, but the coefficients of cross-interaction terms such as  $|W_{12}|^2 W_{11}$  are different. In addition, since  $C_1^2$  has contributions at order of  $\varepsilon^2$ , quadratic terms with the amplitude gradients should appear in the spatio-temporal dynamics of amplitude  $W_{11}$ :

$$\begin{aligned} \partial_{\tau_2} W_{11} = & 2q_c^2 [r_2 W_{11} + (\mathbf{n}_1 \cdot \nabla_1)^2 W_{11} - g|W_{11}|^2 W_{11} \\ & - g_h (|W_{12}|^2 + |W_{13}|^2) W_{11} - h_2 U W_{11}] \\ & - 4iq_c h_2 [W_{13}^* (\mathbf{n}_2 \cdot \nabla_1) W_{12}^* + W_{12}^* (\mathbf{n}_3 \cdot \nabla_1) W_{13}^*], \end{aligned} \quad (101)$$

where  $\mathbf{n}_1, \mathbf{n}_2$ , and  $\mathbf{n}_3$  are the unit vectors along the direction of  $\mathbf{q}_1, \mathbf{q}_2$ , and  $\mathbf{q}_3$ , respectively,  $g = (-2h_2^2/Q^2 + (3h_3/2))$ , and  $g_h = 3h_3 - (2h_2^2/(2 - \sqrt{3})Q^2)$ . Combining the dynamics on scales  $\tau_1$  and  $\tau_2$  by  $\varepsilon^2 \times (97) + \varepsilon^3 \times (101)$ , we have

$$\begin{aligned} (\varepsilon \partial_{\tau_1} + \varepsilon^2 \partial_{\tau_2}) \varepsilon W_{11} = & 2q_c^2 [(\varepsilon r_1 + \varepsilon^2 r_2) \varepsilon W_{11} - \varepsilon^2 h_2 W_{12}^* W_{13}^* + \varepsilon^3 (\mathbf{n}_1 \cdot \nabla_1)^2 W_{11} \\ & - \varepsilon^3 g |W_{11}|^2 W_{11} - \varepsilon^3 g_h (|W_{12}|^2 + |W_{13}|^2) W_{11} - h_2 U W_{11}] \\ & - 4iq_c h_2 \varepsilon^3 [W_{13}^* (\mathbf{n}_2 \cdot \nabla_1) W_{12}^* + W_{12}^* (\mathbf{n}_3 \cdot \nabla_1) W_{13}^*]. \end{aligned} \quad (102)$$

Using relations (15)–(17), Eq. (102) can be rescaled to an equation of original variables.

Equations for  $W_{12}$  and  $W_{13}$  are obtained by permuting subscripts. Similar amplitude equations for hexagonal planforms have been investigated by Brand (1989), Gunaratne et al. (1994), Kuznetsov et al. (1995) in different contexts.

4. At order of  $\varepsilon^4$ , collecting terms independent of rapid variables, one obtains

$$\partial_{\tau_2} U = h_c \nabla_1^2 U + 2h_2 \nabla_1^2 (|W_{11}|^2 + |W_{12}|^2 + |W_{13}|^2). \quad (103)$$

Since no such terms can be collected on time scale  $\tau_1$ , Eq. (103) alone gives the complete dynamics of the large scale mode. Returning to the unscaled variables and rescaling  $t \rightarrow t/2q_c^2$ , we obtain Eqs. (33)–(34).

## References

- Bracewell, R., 1999. The Hankel transform. In: *The Fourier Transform and its Applications*, third ed. McGraw-Hill, New York, p. 244.
- Brand, H.R., 1989. Envelop equations near the onset of a hexagonal pattern. *Prog. Theor. Phys. Suppl.* 99, 442.
- Busse, F.H., 1967. On the stability of two-dimensional convection and its relation to an extremum principle. *J. Fluid Mech.* 30, 625.
- Cahn, J.W., Hilliard, J.E., 1958. Free energy of a nonuniform system, I. Interfacial free energy. *J. Chem. Phys.* 28, 258.
- Cross, M.C., Hohenberg, P.C., 1993. Pattern formation outside of equilibrium. *Rev. Mod. Phys.* 65 (3), 851.
- Glas, F., 1997. Thermodynamics of a stressed alloy with a free surface: coupling between the morphological and compositional instabilities. *Phys. Rev. B* 55, 11277.
- Golovin, A.A., Nepomnyashchy, A.A., Pismen, L.M., 1994. Interaction between short-scale Marangoni convection and long-scale deformational instability. *Phys. Fluids* 6, 34.
- Golovin, A.A., Nepomnyashchy, A.A., Pismen, L.M., 1997. Nonlinear evolution and secondary instabilities of Marangoni convection in a liquid–gas system with deformable interface. *J. Fluid. Mech.* 341, 317.
- Gunaratne, G.H., Ouyang, Q., Swinney, H.L., 1994. Pattern formation in the presence of symmetries. *Phys. Rev. E* 50, 2802.
- Gunaratne, G.H., Ratnaweera, A., Tennekone, K., 1999. Emergence of order in textured patterns. *Phys. Rev. E* 59, 5058.
- Guyer, J.E., Voorhees, P.W., 1998. Morphological stability and compositional uniformity of alloy thin films. *J. Cryst. Growth* 187, 150.
- Haken, H., 1987. *Advanced Synergetics*. Springer, Berlin.
- Hoyle, R.B., 1998. Universal instabilities of rolls, squares and hexagons. In: Tyvand, P.A. (Ed.), *Time-Dependent Non-linear Convection*. Computational Mechanics Publications, Southampton.
- Hu, S., 2006. Characterization of the dynamics of pattern formation and analysis of self-assembly of nanostructure. Ph.D. Thesis, University of Houston.
- Huang, R., 2005. Kinetic wrinkling of an elastic film on a viscoelastic substrate. *J. Mech. Phys. Solids* 53, 63–89.
- Kuznetsov, E.A., Nepomnyashchy, A.A., Pismen, L.M., 1995. New amplitude equation for Boussinesq convection and nonequilateral hexagonal patterns. *Phys. Lett. A* 205, 261.
- Lu, W., Suo, Z., 1999. Coarsening, refining, and pattern emergence in binary epilayers. *Z. Metal.* 90, 956.
- Lu, W., Suo, Z., 2001. Dynamics of nanoscale pattern formation of an epitaxial monolayer. *J. Mech. Phys. Solids* 49, 1937.
- Lu, W., Suo, Z., 2002. Symmetry breaking in self-assembled monolayers on solid surfaces: anisotropic surface stress. *Phys. Rev. B* 65, 085401.
- Manneville, P., 1990. *Dissipative Structures and Weak Turbulence*. Academic, San Diego, CA.
- Matthews, P.C., Cox, S.M., 2000. Pattern formation with a conservation law. *Nonlinearity* 13, 1293.
- Newell, A.C., Whitehead, J.A., 1969. Finite bandwidth, finite amplitude convection. *J. Fluid Mech.* 38, 279.
- Ng, K., Vanderbilt, D., 1995. Stability of periodic domain structures in a two-dimensional dipolar model. *Phys. Rev. B* 52, 2177.
- Palm, E., 1960. On the tendency toward hexagonal cells in steady convection. *J. Fluid Mech.* 8, 183.
- Plass, R., Last, J.A., Bartelt, N.C., Kellogg, G.L., 2001. Nanostructures: self-assembled domain patterns. *Nature* 412, 875.
- Pohl, K., Bartelt, M.C., De La Figuera, J., Bartelt, N.C., Hrbek, J., Hwang, R.Q., 1999. Identifying the forces responsible for self-organization of nanostructures at crystal surfaces. *Nature* 297, 238.
- Pomeau, Y., Manneville, P., 1980. Wavelength selection in cellular flow. *Phys. Lett. A* 75, 296.
- Segel, L., 1969. Distant side-walls cause slow amplitude modulations of cellular convection. *J. Fluid Mech.* 38, 203.
- Suo, Z., Lu, W., 2000. Forces that drive nanoscale self-assembly on solid surface. *J. Nano. Res.* 2, 233.
- Suo, Z., Lu, W., 2001. Self-organizing nanophases on a solid surface. In: Chuang, T.J. (Ed.), *Multi-scale Deformation and Fracture in Material and Structures*. Kluwer Academic Publisher, Dordrecht.
- Thibos, L.N., 2003. *Fourier Analysis for Beginners*, third ed. Digitally published by the Visual Sciences Group, webpage: (<http://www.research.opt.indiana.edu/Library/FourierBook/title.html>).

- Umezawa, K., Nakanishi, S., Yoshimura, M., Ojima, K., Ueda, K., Gibson, W.M., 2001. Ag/Cu(111) surface structure and metal epitaxy by impact-collision ion-scattering spectroscopy and scanning tunneling microscopy. *Phys. Rev. B* 63, 35402.
- Wahlström, E., Ekvall, I., Olin, H., Lindgren, S., Walldén, L., 1999. Observation of ordered structures for S/Cu(111) at low temperature and coverage. *Phys. Rev. B* 60, 10699.
- Walgraef, D., 1997. *Spatio-Temporal Pattern Formation*. Springer, New York.
- Whitesides, G.M., Grzybowski, B., 2002. Self-assembly at all scales. *Science* 295, 2148.